EFFECT OF RADIAL FINS ON NATURAL CONVECTION BETWEEN HORIZONTAL CIRCULAR AND SQUARE CYLINDERS

Iman Jafari, Hossein Mahdavy-Moghadam, Mohammad Taeibi-Rahni,
Morteza Dayyan

Department of Mechanical and Aerospace Engineering, Science and Research Branch, Islamic Azad University, Tehran,
Iran; e-mail: morteza.dayyan@gmail.com

Seyyed Mostafa Seyyedi

Department of Mechanical Engineering, Babol University of Technology, Babol, Iran

In this paper, the effects of the number and arrangement of radial fins on laminar natural convection between horizontal circular and square cylinders has been investigated numerically with the lattice Boltzmann method. The Rayleigh number is varied from $\mathrm{Ra} = 10^3 - 10^6$), the number of fins $(N = 2 - 8)$ and the Prandtl number $(\mathrm{Pr} = 0.7)$. The local Nusselt number profiles over the outer and inner cylinders and the average Nusselt number over the top, bottom and side walls of the outer cold square cylinder are obtained. The temperature and streamline contours are also depicted to investigate the heat and fluid flow behavior inside the computational domain.

Keyword: radial fins, natural convection, lattice Boltzmann method, horizontal annulus

Nomenclature

c is the lattice speed; f, $\widetilde{f}$ – particle distribution and post-collision particle distribution function, respectively; g $\widetilde{g}$ – temperature distribution and post-collision temperature distribution function, respectively; g^{neq} – non-equilibrium parts of temperature distribution function; f^{eq}, g^{eq} – equilibrium density distribution function; e_α – discrete velocity; Nu_{loc}, Nu_{ave} – local and averaged Nusselt number, respectively; Pr, Ra – Prandtl (ν/α) and Rayleigh number, respectively; T – temperature; $\mathbf{u}$ – flow velocity, $\mathbf{u}(u,v)$; u, v – x- and y-velocity component, respectively; u_f – fluid velocity near wall; u_w – velocity of solid wall; u_{bf} – imaginary velocity for interpolations; X_b – physical boundary; X_f, X_w – fluid and wall node, respectively; t – time [s].

Greek symbols: α – thermal diffusivity $[\mathrm{m^2 s^{-1}}]$; δt – lattice time step; χ – weight factor; Δ – fraction of the intersected link; υ – kinematic viscosity of the fluid $[\mathrm{m^2 s^{-1}}]$; ρ – density of fluid $[\mathrm{kg\,m^{-3}}]$; τ_υ, τ_s – relaxation time for flow and for temperature, respectively; ω_α – constant factors.

Subscripts: b – boundary; f – fluid; ave – average; loc – local; w – wall.

1. Introduction

The phenomenon of natural convection in enclosures has been a subject of research over the years. Among them, convective heat transfer in horizontal annuli has attracted many attentions in engineering sciences due to its wide applications such as in solar collector-receivers and underground electric transmission cables. Kuhen and Goldstein (1976, 1980) presented experimental and numerical studies of steady-state natural convection heat transfer in horizontal concentric annuli in which the effects of Rayleigh and Prandtl numbers and the aspect ratio were parametrically explored, and the correlating equations were proposed as well. Larson *et al.* (1978) carried

out experimental study of a temperature field around a heated horizontal cylindrical body in an isothermal rectangular enclosure. Kim *et al.* (2008) and Lee and Lee (1981) studied the effect of circular cylinder positions on heat transfer in the range of the Rayleigh number by means of a finite volume method. They found that the existence of local peaks of the Nusselt number along the surfaces of the cylinder and the enclosure is determined by the gap and the thermal plume governed by conduction and the convection. Natural convection between a square outer cylinder and a heated elliptic inner cylinder was investigated by Bararnia *et al.* (2011). Their results showed that streamlines, isotherms, the number, size and formation of the cells strongly depend on the Rayleigh number and the position of the inner cylinder. Shi *et al.* (2006) investigated natural convection heat transfer in a horizontal concentric annulus bounded by two stationary cylinders with different temperatures by means of the finite difference based lattice BGK model for thermal flows. They showed the capability and accuracy of the method for different range of the Rayleigh number. The main objective of the present work is to investigate the effect of the number and arrangement of radial fins along with the Rayleigh number on the heat and fluid flow pattern between a hot inner circular and a cold outer square cylinder.

2.   Numerical procedure

Standard (D2Q9) LBM method is used for both flow and temperature in the present work, see Mohamad (2007).

2.1.   Curved boundary treatment

2.1.1.   Treatment of curved boundary for velocity

For treating velocity and temperature fields with curved boundaries, the method proposed by Yan and Zu (2008) has been used. Figure 1 shows an arbitrary curved wall separating a solid region from the fluid.
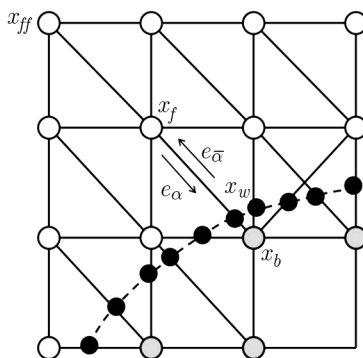
Fig. 1. Layout of lattice nodes and the curved wall boundary

The fraction of the intersected link in the fluid region Δ is defined as

$$\Delta = \frac{|x_f - x_w|}{|x_f - x_b|} \tag{2.1}$$

The post-collision distribution function $\widetilde{f}_{\overline{\alpha}}(x_b, t)$ is defined as

$$\widetilde{f}_{\overline{\alpha}}(x_b, t) = (1 - \chi)\widetilde{f}_{\alpha}(x_f, t) + \chi f_{\alpha}^*(x_b, t) + 2\omega_{\alpha}\rho\frac{3}{c^2}e_{\overline{\alpha}}u_w \tag{2.2}$$

where

$$f_\alpha^*(x_b,t) = f_\alpha^{eq}(x_f,t) + \omega_\alpha \rho(x_f,t)\frac{3}{c^2}e_\alpha(u_{bf} - u_f) \qquad (2.3)$$

and

$$u_{bf} = \begin{cases} u_{ff} = u(x_{ff},t) & \text{if} \quad 0 \leqslant \Delta < \dfrac{1}{2} \\[2mm] \dfrac{1}{2\Delta}(2\Delta - 3)u_f + \dfrac{3}{2\Delta}u_w & \text{if} \quad \dfrac{1}{2} \leqslant \Delta < 1 \end{cases}$$

$$\chi = \begin{cases} \dfrac{2\Delta - 1}{\tau_v - 2} & \text{if} \quad 0 \leqslant \Delta < \dfrac{1}{2} \\[3mm] \dfrac{2\Delta - 1}{\tau_v - \dfrac{1}{2}} & \text{if} \quad \dfrac{1}{2} \leqslant \Delta < 1 \end{cases} \qquad (2.4)$$

In the above, $e_{\overline{\alpha}} \equiv -e_\alpha$, $x_{ff} = x_f + e_{\overline{\alpha}}\delta t$, $u_f \equiv u(x_f,t)$ is the fluid velocity near the wall, $u_w \equiv u(x_w,t)$ is the velocity of the solid wall and u_{bf} is an imaginary velocity for interpolations, and χ is the weight factor that depends on it. Substituting Eq. (2.3) into Eq. (2.2), gives

$$\widetilde{f_{\overline{\alpha}}}(x_b,t) = \widetilde{f}_\alpha(x_f,t) - \chi[\widetilde{f}_\alpha(x_f,t) - \widetilde{f}_\alpha^{eq}(x_f,t)] + \omega_\alpha\rho(x_f,t)\frac{3}{c^2}e_\alpha[\chi(u_{bf} - u_f) - 2u_w] \qquad (2.5)$$

2.1.2. Treatment curved boundary for temperature

Following the work of Yan and Zu (2008), the non-equilibrium parts of temperature distribution function can be defined as

$$g_{\overline{\alpha}}^{neq}(x,t) = g_{\overline{\alpha}}(x,t) - \widetilde{g}_{\overline{\alpha}}(x,t) \qquad (2.6)$$

Thus, the post-collision state function of temperature leads to

$$\widetilde{g}_{\overline{\alpha}}(x,t) = g_{\overline{\alpha}}^{eq}(x,t) + \left(1 - \frac{1}{\tau_s}\right)g_{\overline{\alpha}}^{neq}(x,t) \qquad (2.7)$$

Obviously, to calculate the value of $\widetilde{g}_{\overline{\alpha}}(x_b,t)$, both $g_{\overline{\alpha}}^{eq}(x_b,t)$ and $g_{\overline{\alpha}}^{neq}(x_b,t)$ are needed. In Eq. (2.7), the equilibrium part is defined as

$$g_{\overline{\alpha}}^{eq}(x_b,t) = \omega_{\overline{\alpha}}T_b^*\left(1 + \frac{3}{c^2}e_{\overline{\alpha}}u_b^*\right) \qquad (2.8)$$

where T_b^* is defined as

$$T_b^* = \begin{cases} T_{b1} & \text{if} \quad \Delta \geqslant 0.75 \\ T_{b1} + (\Delta - 1)T_{b2} & \text{if} \quad \Delta < 0.75 \end{cases} \qquad (2.9)$$

where

$$T_{b1} = \frac{1}{\Delta}[T_w + (\Delta - 1)T_f] \qquad T_{b2} = \frac{1}{1+\Delta}[2T_w + (\Delta - 1)T_{ff}] \qquad (2.10)$$

and u_b^* is defined as function of

$$u_b^* = \begin{cases} u_{b1} & \text{if} \quad \Delta \geqslant 0.75 \\ u_{b1} + (\Delta - 1)u_{b2} & \text{if} \quad \Delta < 0.75 \end{cases} \qquad (2.11)$$

where

$$u_{b1} = \frac{1}{\Delta}[u_w + (\Delta - 1)u_f] \qquad u_{b2} = \frac{1}{1+\Delta}[2u_w + (\Delta - 1)u_{ff}] \qquad (2.12)$$

The non-equilibrium part in Eq. (2.6) is defined as

$$g_\alpha^{neq}(x_b,t) = \Delta g_\alpha^{neq}(x_f,t) + (1 - \Delta)g_\alpha^{neq}(x_{ff},t) \qquad (2.13)$$

2.2. Grid study and validation of the present lattice Boltzmann code

To test and assess grid independency of the solution scheme, numerical experiments have been performed for grid sizes of 201×201, 251×251, 301×301 and 351×351. Various mesh combinations were examined for the case of $\text{Ra} = 10^6$ at $N = 8$. The present code was tested for grid independence by calculating the average Nusselt number on the outer cold walls. As seen in Table 1, a grid mesh of 301×301 is adequate to describe the heat transfer processes correctly. The convergence criterion for the termination of all computations is

$$\max_{grid} \left| \sqrt{(u^2 + v^2)^{n+1}} - \sqrt{(u^2 + v^2)^n} \right| \leqslant 10^{-6} \qquad \max_{grid} |T^{n+1} - T^n| \leqslant 10^{-6} \qquad (2.14)$$

Table 1. Results of the average Nusselt number on the outer cold walls for the grid test for $\text{Ra} = 10^6$, $N = 8$

Mesh	Nu_{ave}
201×201	2.4886
251×251	2.5135
301×301	2.5053
351×351	2.5053

Table 2 and Fig. 2 illustrate the comparison between the calculated average Nusselt numbers of Kim *et al.* (2008) and the present results. These comparisons illustrate an excellent agreement between the present calculations and the previous works.

Table 2. Comparison of the average Nusselt number along the hot surface obtained by the present solution with the previous work by Kim *et al.* (2008) for different Rayleigh numbers at $\text{Pr} = 0.7$

Ra	Present	Kim *et al.* (2008)
10^3	3.454	3.414
10^6	9.343	9.39
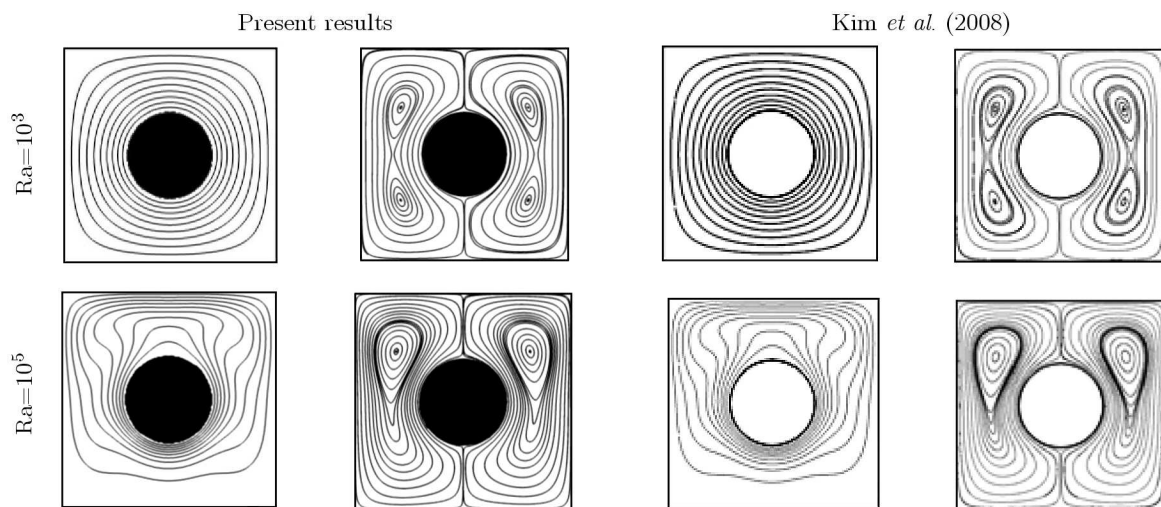
Fig. 2. Comparison of the present solution with the previous work by Kim *et al.* (2008) for different Rayleigh numbers at $\text{Pr} = 0.7$

3.   Physical model and boundary conditions

The computational domain in the present investigation consists of a hot inner circular and a cold outer square cylinder. The working fluid within the annulus is air with $Pr = 0.7$. Figure 3 shows different cases considered in this investigation. Figures 3a and 3b depict the annulus with two horizontal and vertical fins. In other cases, the numbers of radial fins are 4, 6 and 8, respectively. Temperature of the fins in all cases is equal to the hot inner cylinder.
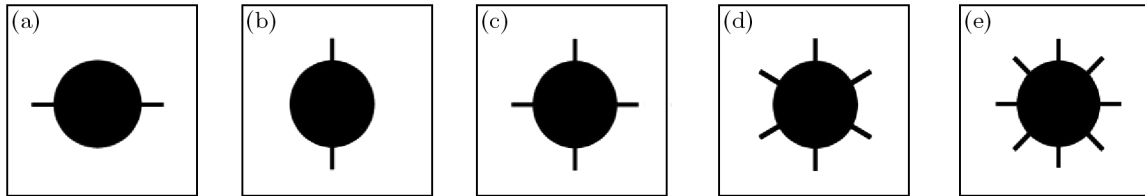
Fig. 3. A scheme the considered problem with various numbers of radial fins

4.   Results and discussion

The LBM method is implemented to obtain the heat and flow distribution inside the computational domain. The calculations are carried out for a constant Prandtl number ($Pr = 0.7$). The Rayleigh number varies from 10^3 to 10^6. The local Nusselt number Nu_{loc} over each surface is defined as

$$Nu_{loc} = -\frac{\partial \theta}{\partial n}\Big|_{wall} \tag{4.1}$$

where n denotes the external unit normal to the wall surface. The thermal heat transfer to or from the walls is characterized by the average Nusselt number Nu_{ave}

$$Nu_{ave} = \frac{1}{W} \int_0^W Nu_{loc}\, ds \tag{4.2}$$

Figure 4 shows the streamlines and isotherm for annulus with two horizontal fins. For low Rayleigh numbers ($Ra = 10^3$, 10^4), the isotherms are uniformly distributed between the inner and outer cylinders. In addition, the isotherms take shape of the surfaces, which is characteristic for the conduction dominant regime. With an increase in the Rayleigh number up to 10^5 gradually, a thermal plume appears over the hot circular cylinder, which shows that the convective heat transfer mode becomes comparable to the conduction. For higher Rayleigh numbers ($Ra = 10^5$, 10^6), the isotherms are denser beneath the cylinder, which results in a higher temperature gradient at this area. The streamlines show that the existence of the horizontal fin leads to the same flow pattern at different Rayleigh numbers. For all Ra, two pair vortices formed inside the cavity; as the Rayleigh number increases, the center of these vortices moves upwards and the size of the two lower vortices decreases considerably.

The local Nusselt number profiles over the inner and outer cylinders are shown in Figs. 5a and 5b. Figure 5a indicates that the maximum Nusselt number occurs at the poin A, where the thermal plume strongly impinges the cold top wall, and then it decreases as we move towards the point B. As we move from the point B to S, the local Nusselt number again enhances, because hot the fluid could approach to the vicinity of the could surface. Moving towards the point C, again the local Nusselt diminishes, and by passing this point, the profiles gradually enhance. It should be noted that with an increase in the Rayleigh number, the local Nusselt number decreases over the bottom cold wall (C-D), due to the point that in this region the
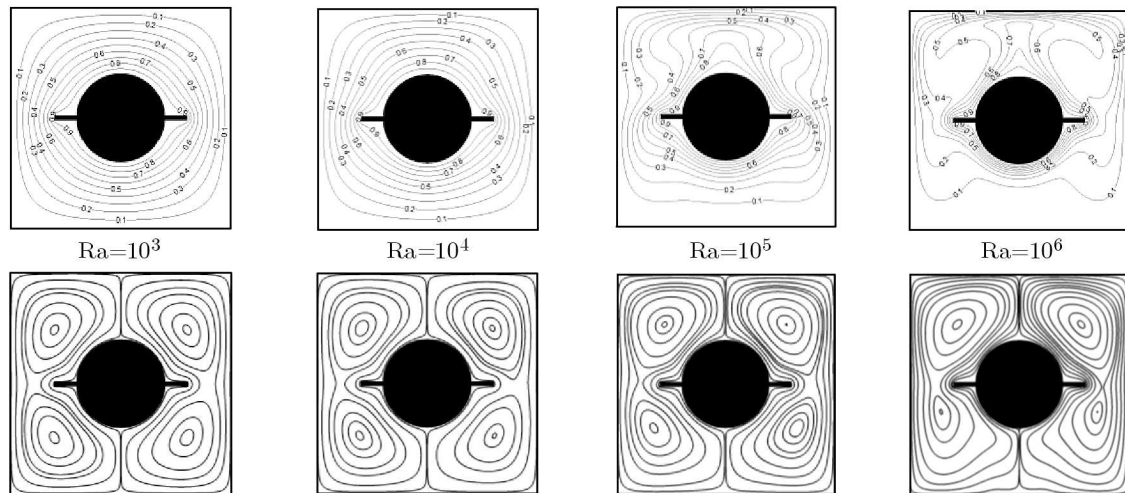
Fig. 4. Streamlines and isotherms two horizontal fins arrangement, and $Ra = 10^3$-10^6

hot surface located over the cold one, hence the increase in the Rayleigh number confines the isotherms to the vicinity of the upper hot surface and leads to a smaller value of the local Nusselt number. Variation of the local Nusselt number over the surface of the hot cylinder is depicted in Fig. 5b. As seen, the value of Nu_{loc} is small above the inner cylinder, where the existence of thermal plume causes a thicker thermal boundary layer. As we approach to the radial fin, Nu_{loc} decreases and then increases, and reaches to its maximum value at $\phi = 180°$.
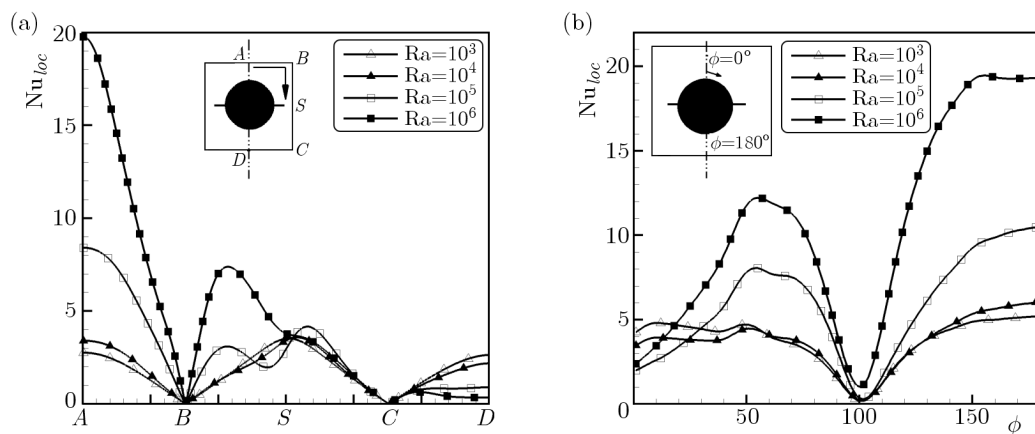
Fig. 5. Local Nusselt profiles for the two-fin horizontal arrangement over the (a) cold outer cylinder and (b) hot inner circular cylinder at various Rayleigh numbers

Figure 6 shows the isotherms and streamlines for the two-fin vertical arrangement. The isotherms are nearly the same as those of horizontal arrangement, except for that the temperature gradient beneath the hot cylinder is more distributed because the fins do not suppress the fluid flow. The streamlines show that at low Rayleigh numbers, two pair vortices exist inside the enclosure. As the Rayleigh increases, the size of two lower vortices decrease gradually, and finally at $Ra = 10^6$, only the two upper vortices remain within the enclosure.

Figures 7a and 7b depict the local Nusselt number profiles for the two-fin vertical arrangement. The variation of the local Nusselt number over the outer cylinder is nearly the same as those of the two-fin horizontal arrangement. Figure 7b demonstrates that Nu_{loc} over the inner cylinder enhances with an increase in the tangential angle and reaches its maximum value at the lower half of the circular cylinder.
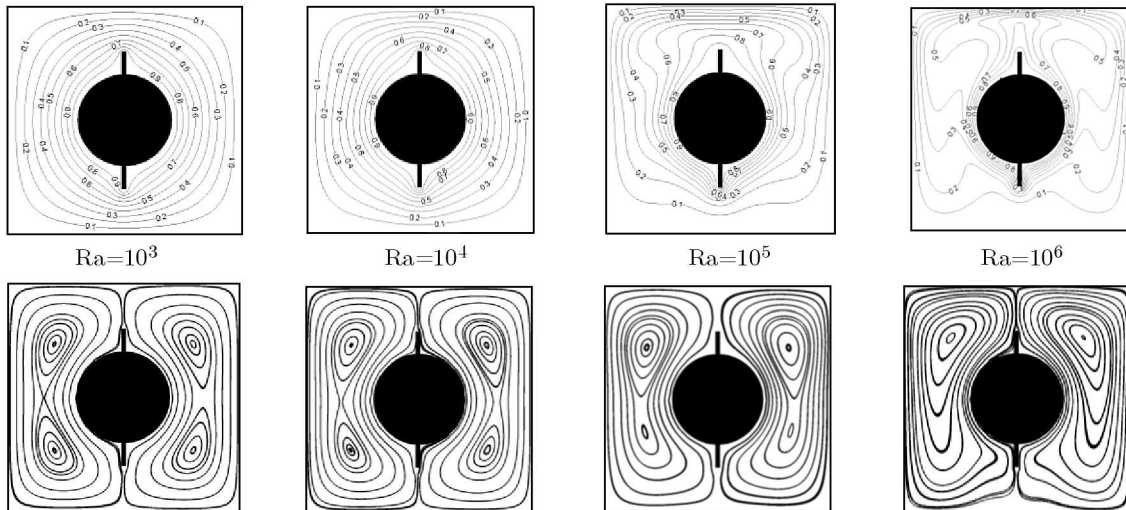
Fig. 6. Streamlines and isotherms for the two-fin vertical arrangement and Ra = 10^3-10^6
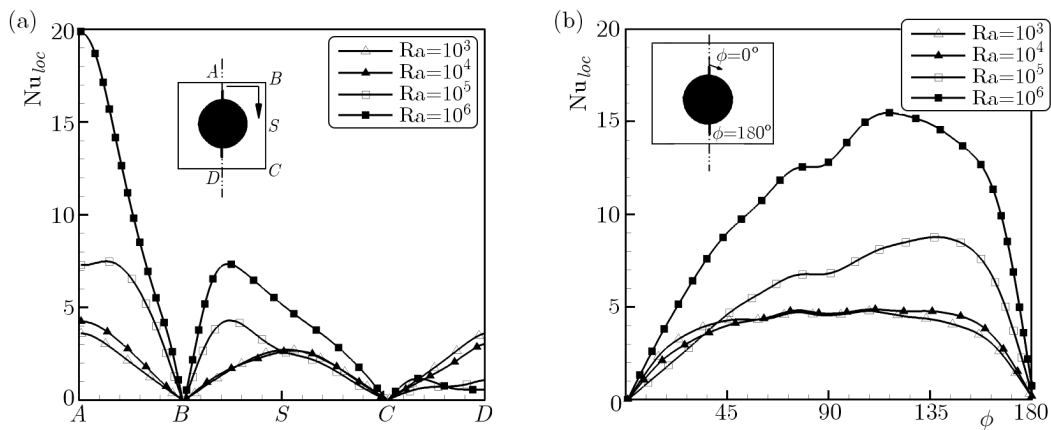
Fig. 7. Local Nusselt profiles for the two-fin vertical arrangement over the (a) cold outer cylinder and (b) hot inner circular cylinder at various Rayleigh numbers

The isotherms and streamlines for the four-fin arrangement are shown in Fig. 8. The isotherms show that as the Rayleigh number increases, the convection heat transfer mechanism becomes much more pronounced, and a thermal plume forms over the hot inner cylinder. The flow pattern for this case is similar to that of the two horizontal fine arrangements. The streamlines depict that for all Rayleigh numbers four eddies exist inside the cavity. With an increase in the Rayleigh number, the size of lower vortices decreases considerably while the size of upper ones remains nearly constant.

The local Nusselt number profiles (Figs. 9a and 9b) show that the local Nusselt number over the hot surface has two local maximum values; the first one near $\phi = 45°$ and the other one at $\phi = 135°$.

Figure 10 depicts the isotherms and streamlines for the six-fin arrangement for Ra = 10^3-10^6. As the Rayleigh number increases to Ra = 10^5, a thermal plume starts to form above the hot circular cylinder, which is similar to the previous cases. The isotherms for Ra = 10^6 demonstrate that at this Rayleigh number, the temperature distribution pattern is different from those of previous cases. Two plumes form above the two-side radial fins at the upper part of enclosure which impinges the hot fluid to the upper wall; the cold returning fluid from the upper wall also forms a reverse thermal plume at the middle of the enclosure. The streamlines show the existence of three pairs of vortices for Ra $\leqslant 10^5$ inside the enclosure. At Ra = 10^6 the fluid flow
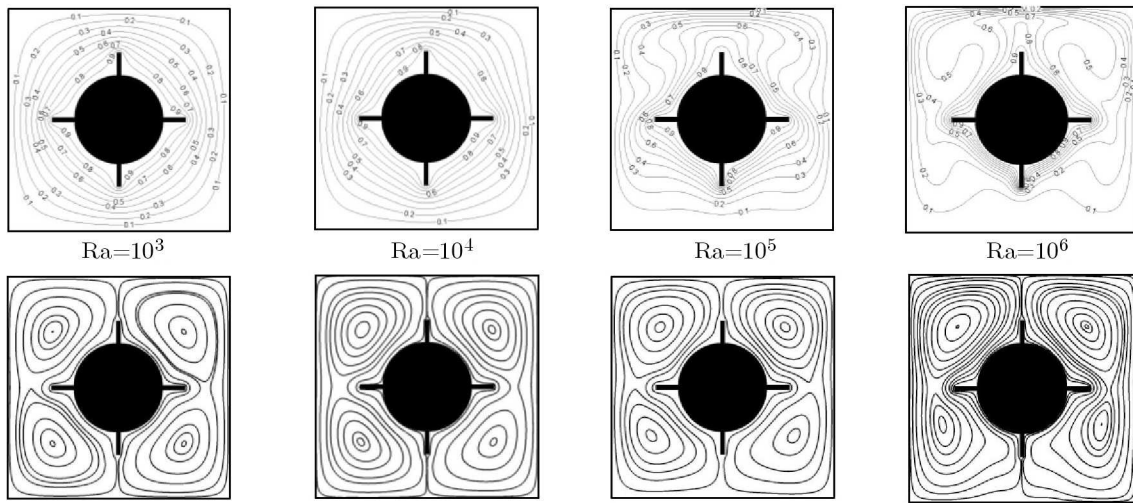
Fig. 8. Streamlines and isotherms for the four-fin arrangement and $Ra = 10^3$-10^6
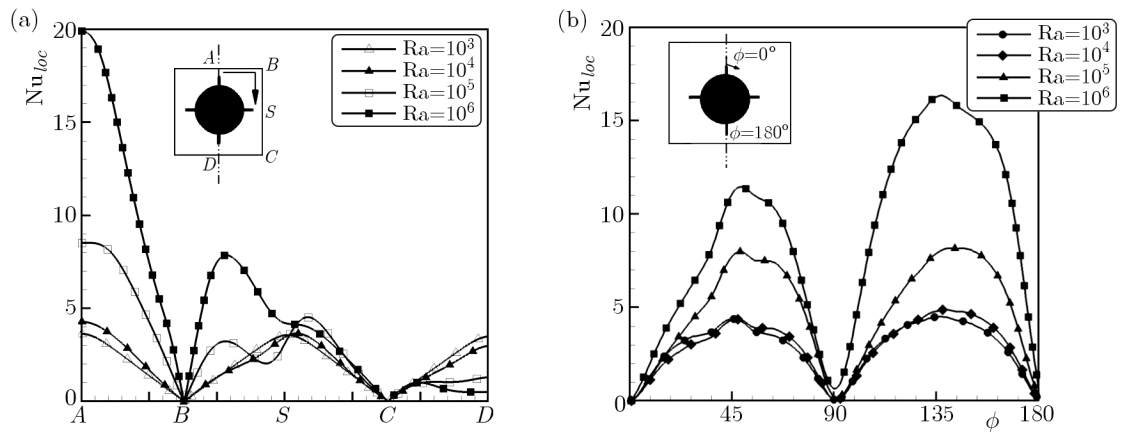
Fig. 9. Local Nusselt profiles for the four-fin horizontal arrangement over the (a) cold outer cylinder and (b) hot inner circular cylinder at various Rayleigh numbers
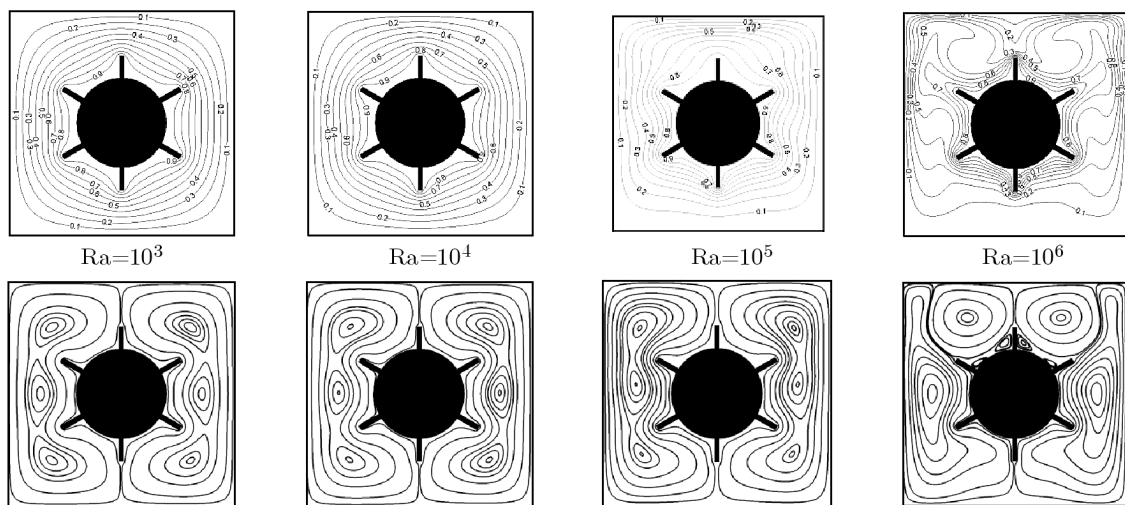
Fig. 10. Streamlines and isotherms for the six-fin arrangement and $Ra = 10^3$-10^6

is characterized by two pairs of vortices inside the cavity; a pair of vortices near the side walls of the enclosure and the other pair above the hot circular cylinder. The streamlines also indicate the existence of small eddies at the top of the hot cylinder in the area confined with radial fins.

The local Nusselt number profile over the hot inner and cold outer cylinders are shown in Fig. 11. As seen in Fig. 11a, for $Ra = 10^6$, the local Nusselt number experiences a local minimum value; it is due to the existence of the reverse thermal plume which makes the temperature gradient over the cold surface decrease at the point A. The figure also shows that the value of Nu_{loc} is higher between points B and C at $Ra = 10^6$ because of the formation of two thermal plumes near the side walls. The local Nusselt profile over the inner cylinders shows three local maximum. Moreover, the value of these local maximum numbers is considerably less than those of the two- and four-fin arrangements. This decrement occurs because the radial fins over the inner cylinder confine the hot fluid near the inner cylinder which results in a less temperature gradient and the Nusselt number in this area. The temperature contours and streamlines for the eight-fin arrangement is shown in Fig. 12. It can be seen that the temperature distribution characteristic for this case is the same as that of the six-fin arrangement for various Rayleigh numbers. The streamlines show that two-pair vortices exist inside the cavity at low Rayleigh numbers i.e. $Ra = 10^3$, 10^4. With an increase in the Rayleigh number, the secondary vortices form above the inner cylinder and between the radial fins in this region.
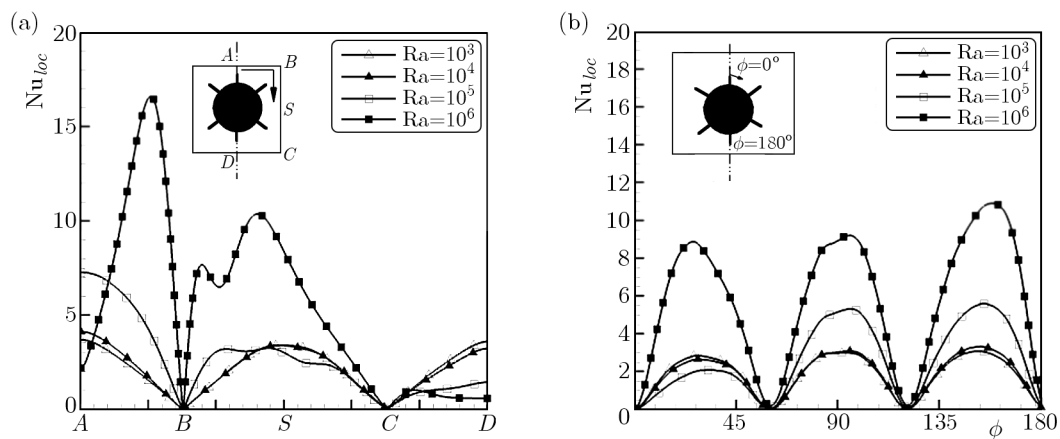
Fig. 11. Local Nusselt profiles for the six-fin horizontal arrangement over the (a) cold outer cylinder (b) hot inner circular cylinder at various Rayleigh numbers
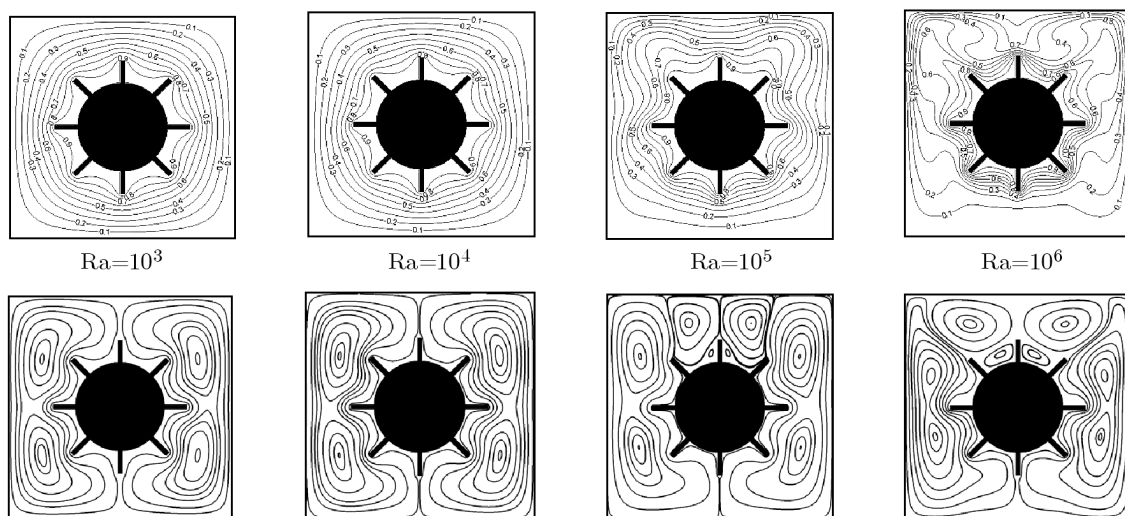
Fig. 12. Streamlines and isotherms for the eight-fin arrangement and $Ra = 10^3$-10^6

Figure 13 shows that the local Nusselt number profiles over the inner and outer cylinders are the same as those of the six-fin arrangement except the number of local maximum value over the hot inner cylinder.
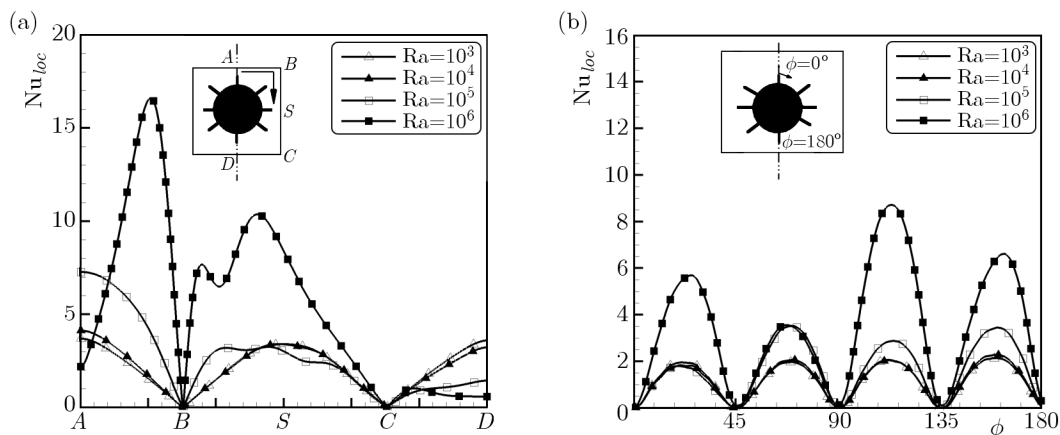
Fig. 13. Local Nusselt profiles for the eight-fin horizontal arrangement over the (a) cold outer cylinder and (b) hot inner circular cylinder at various Rayleigh numbers

The influence of the Rayleigh number and fin arrangement on heat transfer has been more highlighted in Fig. 14. It is observed that the overall heat transfer drastically depends on the arrangement of fins, and the average Nusselt number decreases with rise of the number of fins. This is because of when the fin arrangement changes, the number of fins over the inner cylinders is increased, so it decreases fluid convection. It is also seen that the effect of fins decreases when the Rayleigh number increases. This means that at higher Rayleigh numbers, the heat transfer rate is more dependent on the number of fins over the inner cylinder.
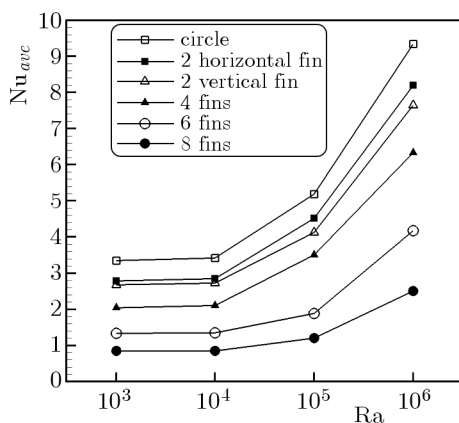
Fig. 14. Variation of the average Nusselt number over the inner cylinders for various arrangements and numbers of radial fins

5.   Conclusion

The lattice Boltzmann method is used to investigate the effects of the number and arrangement of radial fins on laminar natural convection between horizontal circular and square cylinders in this study. The results are depicted in terms of the local and average Nusselt profiles over the walls and the inner cylinders. The temperature and streamline contours are also depicted in this study. The obtained results clearly indicate that the number and arrangement of radial fins over the inner cylinder as well as the Rayleigh number have remarkable effects on the streamlines,

temperature contours and vortex formation in the enclosure. Besides, the temperature contour and streamlines for the six-fin and eight-fin arrangements showed different behavior from those of the two-fin and four-fin arrangements. The results show that as the Rayleigh number increases, the Nusselt number is also increased. However, over the inner cylinder, the averaged Nusselt number is decreased as the number of fins increases. Note that the maximum of this averaged Nusselt number is for the case where no fins are used.

References

1. BARARNIA H., SOLEIMANI S., GANJI D.D., 2011, Lattice Boltzmann simulation of natural convection around a horizontal elliptic cylinder inside a square enclosure, *International Communications in Heat and Mass Transfer*, **38**, 1436-1442

2. KIM B.S., LEE D.S., HA M.Y., YOON H.S., 2008, A numerical study of natural convection in a square enclosure with a circular cylinder at different vertical locations, *International Journal of Heat and Mass Transfer*, **51**, 1888-1906

3. KUHEN T.H., GOLDSTEIN R.J., 1976, Correlating equations for natural convection heat transfer between horizontal circular cylinders, *International Journal of Heat and Mass Transfer*, **19**, 1127-1134

4. KUHEN T.H., GOLDSTEIN R.J., 1980, A parametric study of Prandtl number and diameter ratio effects on natural convection heat transfer in horizontal cylindrical annuli, *Journal of Heat Transfer*, **102**, 768-770

5. LARSON D.W., GARTLING D.K., SCHIMMEL W.P., 1978, Natural convection studies in nuclear spent-fuel shipping casks: computation and experiment, *J. Energy*, **2**, 3, 147-154

6. LEE J.H., LEE T.S., 1981, Natural convection in the annuli between horizontal cofocal elliptic cylinders, *International Journal of Heat and Mass Transfer*, **24**, 1739-1742

7. MOHAMAD A.A., 2007, Applied lattice Boltzmann method for transport phenomena, momentum, heat and mass transfer, *Canadian Journal of Chemical Engineering*, **85**, 946-947

8. SHI Y., ZHAO T.S., GUO Z.L., 2006, Finite diference-based lattice Boltzmann simulation of natural convection heat transfer in a horizontal concentric annulus, *Computers and Fluids*, **35**, 1-15

9. YAN Y.Y., ZU Y.Q., 2008, Numerical simulation of heat transfer and fluid flow past a rotating isothermal cylinder – a LBM approach, *International Journal of Heat and Mass Transfer*, **51**, 2519-2536